Regulation by Chemokines of Circulating Dendritic Cell Precursors, and the Formation of Portal Tract–associated Lymphoid Tissue, in a Granulomatous Liver Disease

By Hiroyuki Yoneyama,*‡ Kenjiro Matsuno,‖ Yanyun Zhang,* Masako Murai,*‡ Meiji Itakura,* Sho Ishikawa,* Go Hasegawa,§ Makoto Naito,§ Hitoshi Asakura,‡ and Kouji Matsushima*

*From the *Department of Molecular Preventive Medicine, School of Medicine and Core Research for Evolutional Science and Technology (CREST), The University of Tokyo, Bunkyoku, Tokyo 113-0033, Japan; the ‡Third Department of Internal Medicine and the §Second Department of Pathology, Niigata University School of Medicine, Niigata-shi, Niigata 951-8122, Japan; and the ‖Department of Anatomy II, Kumamoto University School of Medicine, Kumamoto 860-0811, Japan*

Abstract

We have studied the recruitment and roles of distinct dendritic cell (DC) precursors from the circulation into *Propionibacterium acnes*–induced granulomas in mouse liver. During infection, $F4/80^{-}B220^{-}CD11c^{+}$ DC precursors appeared in the circulation, migrated into the perisinusoidal space, and matured within newly formed granulomas. Recruited DCs later migrated to the portal area to interact with T cells in what we term "portal tract–associated lymphoid tissue" (PALT). Macrophage inflammatory protein 1α attracted blood DC precursors to the sinusoidal granuloma, whereas secondary lymphoid organ chemokine (SLC) attracted mature DCs to the newly identified PALT. Anti-SLC antibody diminished PALT expansion while exacerbating granuloma formation. Therefore, circulating DC precursors can migrate into a solid organ like liver, and participate in the granulomatous reaction in response to specific chemokines.

Key words: dendritic cells • CC chemokine • migration • portal system • inflammation

Introduction

Dendritic cells (DCs)[1] are the most potent initiators of immunity. Therefore, the mobilization of DCs is pivotal to immune surveillance (1). Two established migration pathways of DCs are known: DC precursors, which enter the peripheral tissues from the bloodstream to act as first-line sentinels, and antigen-transporting DCs, which move from the tissues to the regional LNs to promote immune response (2–7). The trafficking of the latter is regulated by the CC chemokine receptor (CCR)7–secondary lymphoid organ chemokine (SLC) system operating at least in part through afferent lymphatics (6, 7). On the other hand, DC precursors may transmigrate the blood vessel endothelia to enter the tissues through locally produced chemokines (3–5). In severe inflammatory conditions, accelerated traffic of DC precursors from the bloodstream has been suggested in the lung (3, 8), heart, skin, kidney (9–11), and liver (12–14). More work is needed to identify DC precursors in the circulation and to understand their development in vivo.

Chemokines have been revealed to play central roles in immunity by regulating the mobilization of immune cells, not only in inflammatory but also steady-state conditions (15–17). Selective recruitment of leukocytes to sites of inflammation and immune responses is based on the selective expression of specific chemokine receptors on each type of leukocyte. Recent investigations have highlighted the regulatory role of chemokines in immune cell dynamics within lymphoid organs (6, 7, 16–19). Immune cells are systematically concentrated within clearly defined "functional compartments", and their distribution is strictly regulated by chemokines (16–19). Molecular-based investigations are therefore now linked to a functional histology.

Address correspondence to K. Matsushima, Department of Molecular Preventive Medicine, School of Medicine, The University of Tokyo, 7-3-1 Hongo, Bunkyoku, Tokyo 113-0033, Japan. Phone: 81-3-5841-3431; Fax: 81-3-5684-2297; E-mail: koujim@m.u-tokyo.ac.jp

[1]*Abbreviations used in this paper:* ALT, alanine transferase; BrdU, 5-bromo-2′-deoxyuridine; CCR, CC chemokine receptor; DC, dendritic cell; FDC, follicular DC; HEV, high endothelial venule; LD, low density; MIP, macrophage inflammatory protein; MLR, mixed leukocyte reaction; NPC, nonparenchymal cell; pAb, polyclonal Ab; PALT, portal tract–associated lymphoid tissue; PNAd, peripheral node addressin; SLC, secondary lymphoid organ chemokine.

J. Exp. Med. © The Rockefeller University Press • 0022-1007/2001/01/35/15 $5.00
Volume 193, Number 1, January 1, 2001 35–49
http://www.jem.org/cgi/content/full/193/1/35

However, compared with lymphoid tissues, functional anatomical sites within other tissues are not well established. Most chemokine studies of peripheral tissues have described the initial event of immune cell extravasation into inflamed tissue. However, as in the case of lymphoid organs, certain compartments should also exist in nonlymphoid tissues, as immune cells do not evenly distribute throughout the tissues even after transmigration.

The liver is engaged in innate host defense. Phagocytic liver macrophages known as Kupffer cells, which directly abut the blood stream, continually screen and capture antigens from the blood (14). A small number of microorganisms from the gut can also be delivered to the liver via the portal vein, making the local host defense system quite important. Thus, the liver is considered to play essential roles in resistance against blood-borne antigens through its special innate defense systems. Uniquely in the liver, Kupffer cells may also trap blood-borne DCs and translocate them into LNs through hepatic sinusoids-lymph pathway (12, 13). Using a *Propionibacterium acnes*–induced granulomatous liver disease model in mice (20), we have now identified circulating DC precursors and investigated their traffic and needs for chemokines. A novel liver-specific immune tissue, portal tract–associated lymphoid tissue (PALT), was also established by this study.

Materials and Methods

Mice and In Vivo Treatment. Specific pathogen-free female C57BL/6 (H-2b, Ly5.2, and Ly5.1), C3H/HeN (H-2k), and BALB/c (H-2d) mice (8–9 wk old) were obtained from CLEA Japan Inc. Osteopetrotic (op/op) mice (4–5 wk old) and their normal littermates (op/+ or +/+) were provided by Dr. M. Takeya (Kumamoto University, Kumamoto, Japan). Op/op mutants were identified by the absence of teeth (21, 22). Mice were injected with heat-killed *P. acnes* (1 mg/100 μl in PBS; American Type Culture Collection 11828) via the tail vein. Granuloma formation was confirmed with hematoxylin and eosin and Azan staining of formalin-fixed 3-μm thick liver sections (20). Hepatocellular damage was determined by serum alanine transferase (ALT) levels (20). For blocking experiments, 500 μg/100 μl in PBS of anti-SLC polyclonal Ab (pAb) or rabbit IgG (Sigma-Aldrich) were administered 0 and 2 d after *P. acnes* injection. For in vivo proliferation assay, mice were injected with 5-bromo-2′-deoxyuridine (BrdU; 500 μg/100 μl PBS; Sigma-Aldrich) 1 h before killing. All animal experiments complied with the standards set out in the guidelines of The University of Tokyo.

Abs. The following anti–mouse mAbs were used: CD3ε (clone; 145-2C11), CD4 (RM4-5), CD8a (53-6.7), LFA-1 (2D7), CD11b (M1/70), CD11c (HL3), CD14 (rmC5-3), CR1 (8C12), CD44 (IM7), B220 (RA3-6B2), intracellular adhesion molecule (ICAM)-1 (3E2), CD86 (GL-1), Thy1.2 (53-2.1), Gr-1 (RB6-8C5), Pan-NK cell (DX5), peripheral node addressin (PNAd) carbohydrate epitope (MECA-79; all from BD PharMingen), F4/80 (CI:A3-1), DEC-205 (NLDC-145), MHC class II (ER-TR3), murine metallophilic macrophages (MOMA-1; all from BMA Biomedicals), CD11c (N418; Serotec), M342 (Dr. R.M. Steinman, Rockefeller University, New York, NY), FDC-M1 (Dr. M.H. Kosco-Vilbois, Geneva Biomedical Research Institute, Geneva, Switzerland), anti–*P. acnes* (Dr. Y. Eishi, Tokyo Medical and Dental University, Tokyo, Japan), and Ly5.2 (AL1-4A2; Dr. T. Kina, Kyoto University, Kyoto, Japan). A rabbit pAb to bovine type IV collagen (LSL Co.) was used to outline hepatic sinusoids (12). As secondary Abs, an alkaline phosphatase (ALP)-labeled anti–rat or rabbit IgG (Jackson ImmunoResearch Laboratories), a horseradish peroxidase–labeled anti–rat Ig (Biosource International), an horseradish peroxidase–labeled goat $F(ab')_2$ to rabbit IgG (Cappel), and an ALP-conjugated anti–hamster IgG (Cedarlane) were used. For macrophage inflammatory protein (MIP)-1α, a goat pAb to anti–MIP-1α (R&D Systems) was used (23). For SLC, we produced rabbit anti–mouse SLC pAb (24, 24a).

Immunostaining. Single or double immunostaining was performed by indirect immunoalkaline phosphatase or immunoperoxidase methods (12). For triple immunostaining, acetone-fixed 6-μm fresh frozen tissue sections were doubly immunostained using 3,3′-diaminobenzidine (DAB; Wako) substrate solution and ALP substrate kit II (Vector blue; Vector Laboratories). After further fixation with 1% glutaraldehyde (Nakarai) in PBS for 9 min, they were reacted with the third Abs to BrdU or *P. acnes* using a BrdU staining kit (Zymed Laboratories) or M.O.M. immunodetection kit (Vector Laboratories), respectively, and were colored red with Vector Red (Vector Laboratories). Slides were counterstained with Mayer's hematoxylin.

Enrichment of DCs from Nonparenchymal Cells. Nonparenchymal cells (NPCs) were prepared as described by Kawada et al. (25), with some modifications. Liver was perfused in situ via the portal vein with liver perfusion medium (LPM; 137 mM NaCl, 5.4 mM KCl, 0.6 mM NaH2PO4, 0.8 mM Na2HPO4, 10 mM Hepes, 3.8 mM CaCl2, 4.2 mM NaHCO3, and 5 mM glucose, pH 7.35) for 10 min, followed by collagenase solution (1 mg/ml in LPM; Wako) for 5 min at 37°C at a flow rate of 4 ml/min. After perfusion, the liver was excised and incubated in collagenase solution containing 20 μg/ml DNase (Boehringer) at 37°C for 30 min with constant stirring. Cell suspensions (5 ml in RPMI 1640 supplemented with 10% heat-inactivated FCS containing 2.5 mM EDTA) were layered onto 5-ml columns of 16.8% Nycodenz (Nycomed Pharma). After centrifugation (2,500 rpm for 20 min at room temperature), the interface was used as NPCs. Flow cytometric immunofluorescence analyses for CD11c, DEC-205, and F4/80 of freshly isolated NPCs were performed and $CD11c^+$ cells were sorted using an Epics Elite ESP cell sorter (Beckman Coulter) as described previously (20, 26).

Low density (LD), DC-enriched cells were prepared as reported by Woo et al. (27), with slight modifications. NPCs (2×10^6/ml) were placed in 10% FCS-RPMI 1640 supplemented with 15 ng/ml GM-CSF (R&D Systems), and cultured overnight (18 h). Nonadherent cells (3 ml in the medium) were layered onto 5-ml columns of 14.5% Nycodenz. After centrifugation (1,850 rpm for 20 min at room temperature), the interface containing LD cells was carefully collected.

Cell Culture. Peripheral blood (0.8 ml) was obtained by cardiac puncture under ether anesthesia. After density separation (Lympholyte-Mouse; Cedarlane), immunofluorescence analyses were performed and $B220^-CD11c^+$ cells were sorted (26). Reanalysis of the sorted population showed purity >99%. Purified $B220^-CD11c^+$ cells (10^5 cells/ml) were incubated in IMDM (GIBCO BRL) supplemented with 20% FCS, penicillin G (100 U/ml), and streptomycin (100 μg/ml) in the presence of GM-CSF (4 ng/ml). Optimal conditions were maintained every 2–3 d by replacing 50% of the medium with fresh medium containing 4 ng/ml GM-CSF. After 5–7 d, the cultured cells were further incubated with TNF-α (50 ng/ml) in addition to GM-CSF on type I collagen-coated plates (IWAKI) for 3–4 d.

Allogeneic Mixed Leukocyte Reaction. The one-way mixed leukocyte reaction (MLR) was performed in 96-well plates using the Premix WST-1 cell proliferation assay system (Takara Biomedicals), according to the manufacturer's instructions. C57BL/6 mouse liver- and spleen-derived LD cells were incubated with mitomycin C (20 μg/ml) for 30 min at 37°C, then cocultured (3×10–3×10^4 cells/100 μl/well) with nylon-wool passed spleen T cells (4×10^5 cells/100 μl/well) from C3H/HeN mice for 72 h. 4 h before the end of culture, WST-1 (20 μl) was added and the absorbance (450–650 nm) was measured. For peripheral blood $B220^-CD11c^+$ cells, highly purified spleen $CD4^+$ T cells from BALB/c mice were used as the responder cells and proliferation was determined using an MTT assay (5 mg/ml, 15 μl/well; Sigma-Aldrich) as described earlier (26).

Reverse Transcription PCR. Total RNA was isolated from liver specimens and 2×10^5 sorted blood or liver $CD11c^+$ cells using RNazol B (Biotex Laboratories, Inc.) and reverse transcribed (20). Thereafter, cDNA was amplified using the ABI 7700 sequence detector system (Applied Biosystems) with a set of primers and probes corresponding to MIP-1α, SLC, CCR1, CCR5, CCR7, and glyceraldehyde-3-phosphate dehydrogenase (GAPDH) as described previously (20, 23, 24). The primers for SLC were: 5′-GGCTATAGGAAGCAAGAACCAAGT-3′ and 5′-TCAGGCTTAGAGTGCTTCCG-3′. The probes were as follows: 5′-CCCATCCCGGCAATCCTGTTCTTA-3′ for SLC, and 5′-ATCACCATCCAAGTGGCCCAGATGGT-3′ for CCR7. Others were as described earlier (20, 23, 24).

Chemotaxis Assay. Freshly isolated PBLs and NPCs (8×10^5/120 μl in RPMI 1640 plus 0.25% BSA) obtained from *P. acnes*–primed mice at day 7 were loaded into murine type IV collagen-coated transwells (3-μm pore size; Becton Dickinson), which were placed in a 24-well tissue culture plate containing 500 μl of the medium supplemented with or without 100 ng/ml of MIP-1α, macrophage-derived chemokine, IFN-γ–inducible protein (IP)-10 (R&D Systems), or SLC (24). After an incubation period of 4 h at 37°C, cells in the bottom of each well were collected and counted with a hemocytometer. After immunostaining for CD11c, the absolute number of migrated $CD11c^+$ cells was determined by multiplying the total migrated cell number by the fraction of $CD11c^+$ population.

DC Trafficking Assay. Freshly isolated PBLs obtained from *P. acnes*–primed Ly5.2 mice at day 5 were incubated with mAb to CD11c for 30 min, followed by goat anti–hamster IgG-labeled magnetic microbeads (20 μl/10^7 cells; Miltenyi Biotech) for 45 min; $CD11c^+$ cells were then isolated using MACS system according to the manufacturer's instructions. The purity of the $CD11c^+$ cell populations was 92% or more as confirmed by immunofluorescence flow cytometry. Isolated $CD11c^+$ cells ($2 \times$

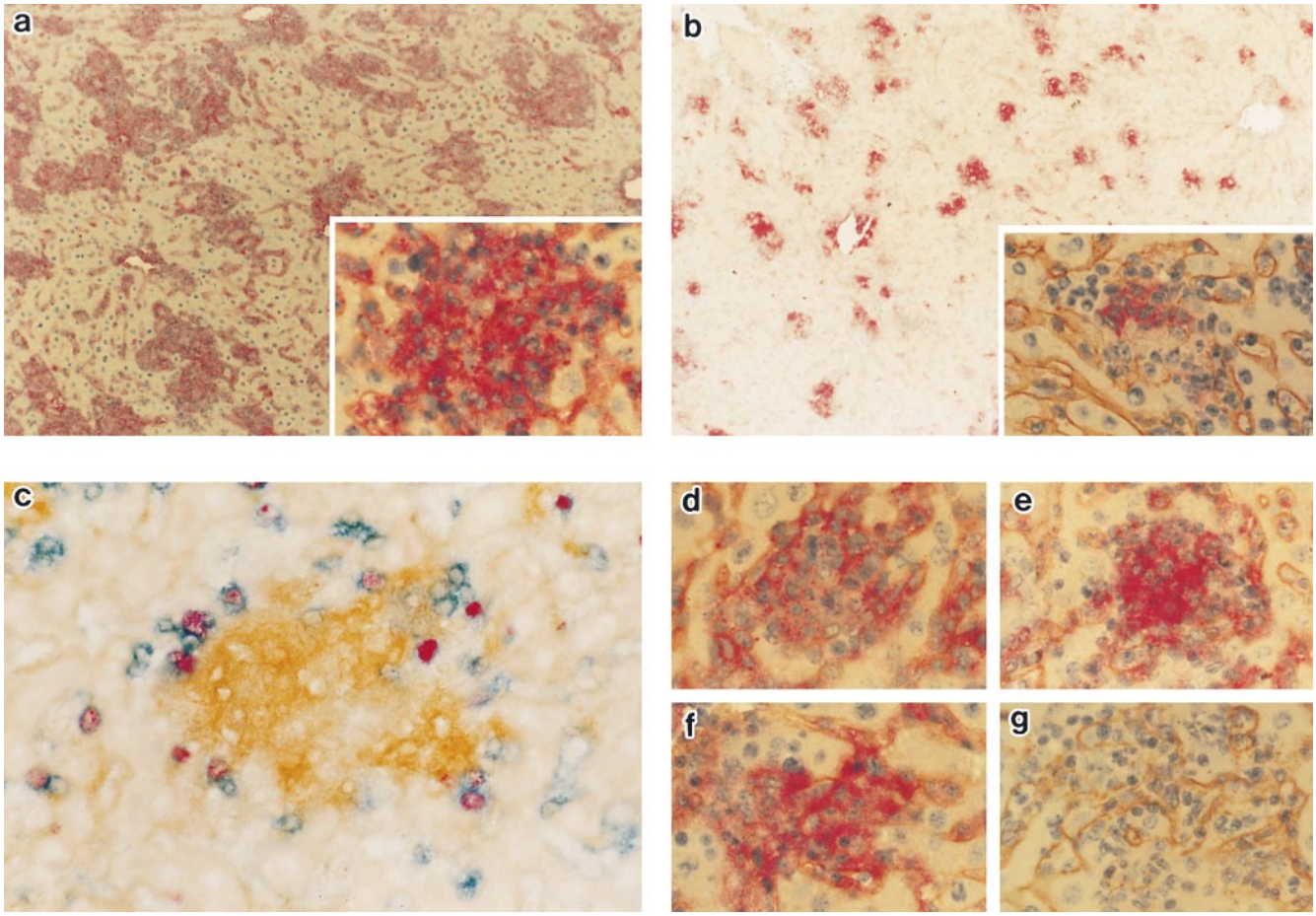

Figure 1. Existence of DCs in hepatic granulomas. Day 7 after *P. acnes* injection. CD11c (a), DEC-205 (b), M342 (d), MHC class II (e), F4/80 (red; f), type IV collagen (brown; a, b, and d–g). (c) DEC-205^+ (brown) cells were clustered with $BrdU^+$(red) $CD4^+$(blue) cells in the granuloma. (g) Type IV collagen alone was a negative control. Original magnifications: (a and b) ×100; (inset, c–g) ×400.

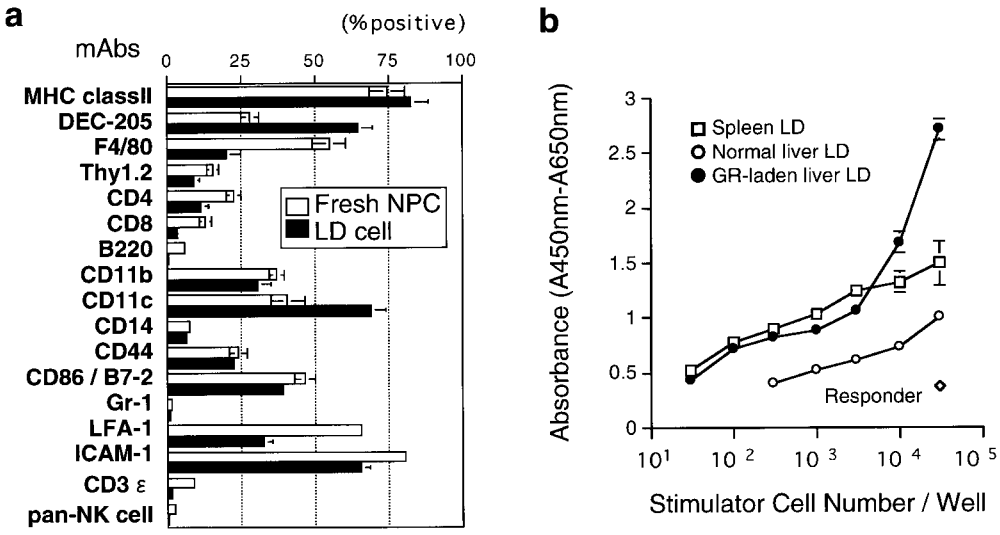

Figure 2. Identification of DCs in hepatic granulomas. (a) Phenotype of granuloma-derived NPCs and LD cells on day 7. (b) Primary allogeneic MLR of granuloma-derived liver LD cells, normal liver LD cells, spleen LD cells, and responder cells alone. Three mice per group and 1,000 total cells/smear were examined. Representative data from six experiments. Mean ± SD (n = 3).

10^6 cells/200 μl in PBS) were injected intravenously into the tail vein of *P. acnes*–primed congeneic Ly5.1 mice at day 5. 1, 6, and 24 h later, recipient liver and hepatic LNs were sampled. After blocking endogenous peroxidase (0.3% hydrogen peroxide in PBS) and avidin/biotin (Avidin/Biotin blocking kit; Vector Laboratories) activity, double immunohistochemical staining for Ly5.2 and B220/CD4 was performed. In some experiments, anti–MIP-1α or SLC pAb and control IgG (200 μg/100 μl PBS) were injected just before cell transfer.

Statistical Analysis. Differences were evaluated using the Student's t test. P values <0.05 were considered to be statistically significant.

Results

Identification of DCs in Hepatic Granulomas. Mice exposed to *P. acnes* by day 7 developed numerous granulomas in the liver (20; Fig. 1, a–g). F4/80$^+$ cells including Kupffer cells and inflammatory macrophages (28) were evenly distributed throughout the granulomas (Fig. 1 f), whereas CD4$^+$ cells localized in the periphery (Fig. 1 c). In addition, cells with the markers of DCs (1, 19, 26), such as CD11c, DEC-205, M342, MHC class II, and CD86, were also distributed within granulomas (Fig. 1, a–e). We then

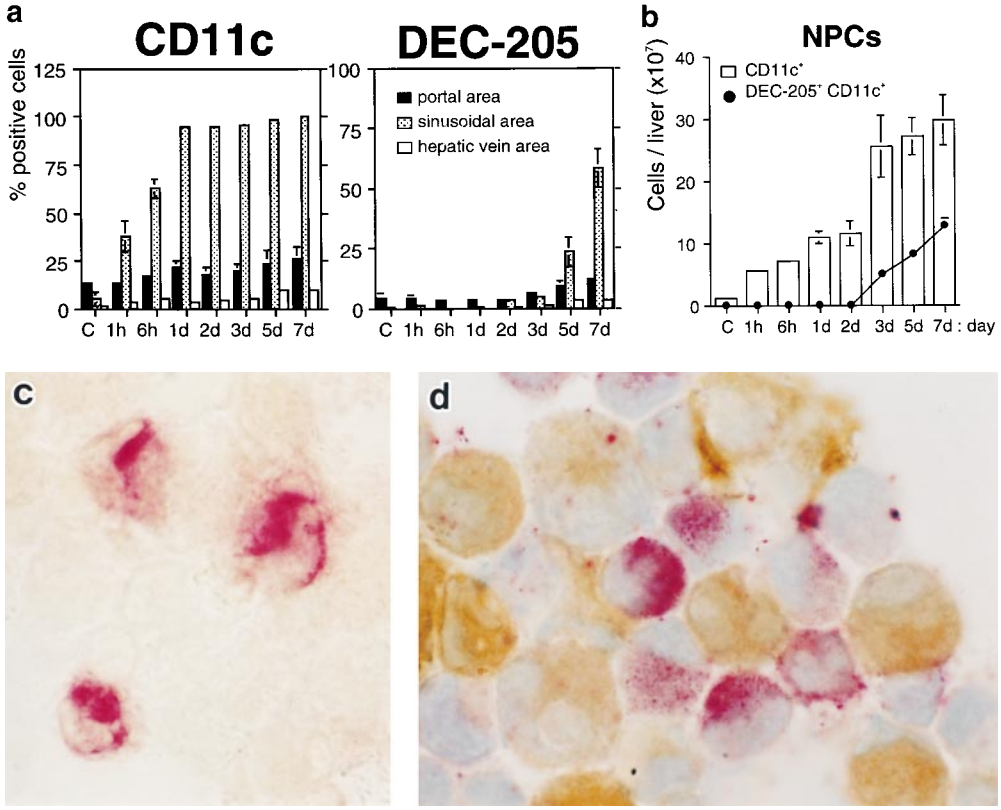

Figure 3. Kinetics of DCs in granuloma formation. (a) 15 mm^2 of stained cryosections were examined for the presence of CD11c$^+$ or DEC-205$^+$ cells. Densely labeled cells were analyzed using a grid micrometer (reference 11). The number of grid intersections overlying positively labeled cells was counted. Final results were presented as the proportion of the number of positive intersections to the total number of grid intersections. (c) Untreated mice as control. (b) The absolute numbers of CD11c$^+$ NPCs (white bars) and DEC-205$^+$CD11c$^+$ NPCs (solid line). Representative data from six independent experiments. Mean ± SD (n = 10). (c) DEC-205$^+$ (red) cells of sorted CD11c$^+$ NPCs on day 4. (d) Cytosmears of NPCs on day 7. Note that CD11c$^+$ cells (red) and F4/80$^+$ macrophages (brown) are clearly distinguishable. Original magnification: (c and d) ×1,000.

investigated LD cells recovered on Nycodenz gradients from the NPC fraction of a granulomatous liver. A majority of LD cells actually had features of DCs, such as an eccentric irregular nucleus and a cytoplasmic membrane with ruffled projections (data not shown). The cells were MHC class II^{high}, CD11c$^+$, DEC-205$^+$, ICAM-1$^+$, CD3ϵ^-, B220$^-$, CD8α^-, Gr-1$^-$, and expressed moderate levels of CD86, LFA-1, and CD11b (Fig. 2 a). In a functional study, they induced considerable proliferation of allogeneic T cells in vitro, compared with normal liver- and spleen-derived LD cells (Fig. 2 b), demonstrating that the granuloma contained functionally mature DCs. Moreover, DEC-205$^+$ cells were in close contact with CD4$^+$ T cells, many of which were in a proliferative stage, as evidenced by in situ BrdU labeling (Fig. 1 c). This suggests that DCs in the granuloma have potent antigen-presenting function and can activate T cells in situ.

Rapid Accumulation of CD11c$^+$ DCs in the P. acnes–primed Liver. Small cell clusters were primarily observed in the sinusoidal, not in the portal, areas by 1 h after *P. acnes* injection. These increased in size by 3 d after *P. acnes* injection, then developed into mature granulomas by day 7. We next investigated the kinetics of DC accumulation in granulomas. In steady state, small numbers of CD11c$^+$ or DEC-205$^+$ interstitial DCs could be found, predominantly within the portal areas (27; Fig. 3 a). However, in the early phase of *P. acnes* injection (1 h–3 d) a new influx of CD11c$^+$ cells appeared in the sinusoidal area and selectively localized in developing granulomas composed of small cell clusters (Fig. 3 a). Subsequently, DEC-205$^+$ cells (Fig. 3 a) as well as CD4$^+$ cells (data not shown) could be found in the developing granuloma beginning at 2–3 d after *P. acnes* treatment. In the late phase (3–7 d), CD11c$^+$ cells were distributed not only within granulomas but also diffusely into the sinusoidal area (Fig. 1 a and Fig. 3 a), whereas DEC-205$^+$ cells were confined to the center of granulomas (Fig. 1 b and Fig. 3 a).

CD11c$^+$ NPCs also increased in number from 1 h after *P. acnes* injection and reached a peak by day 3 (Fig. 3 b). The expression of DEC-205 by CD11c$^+$ NPCs was observed beginning at day 3 and gradually increased in number (Fig. 3, b and c), similar to their distribution pattern

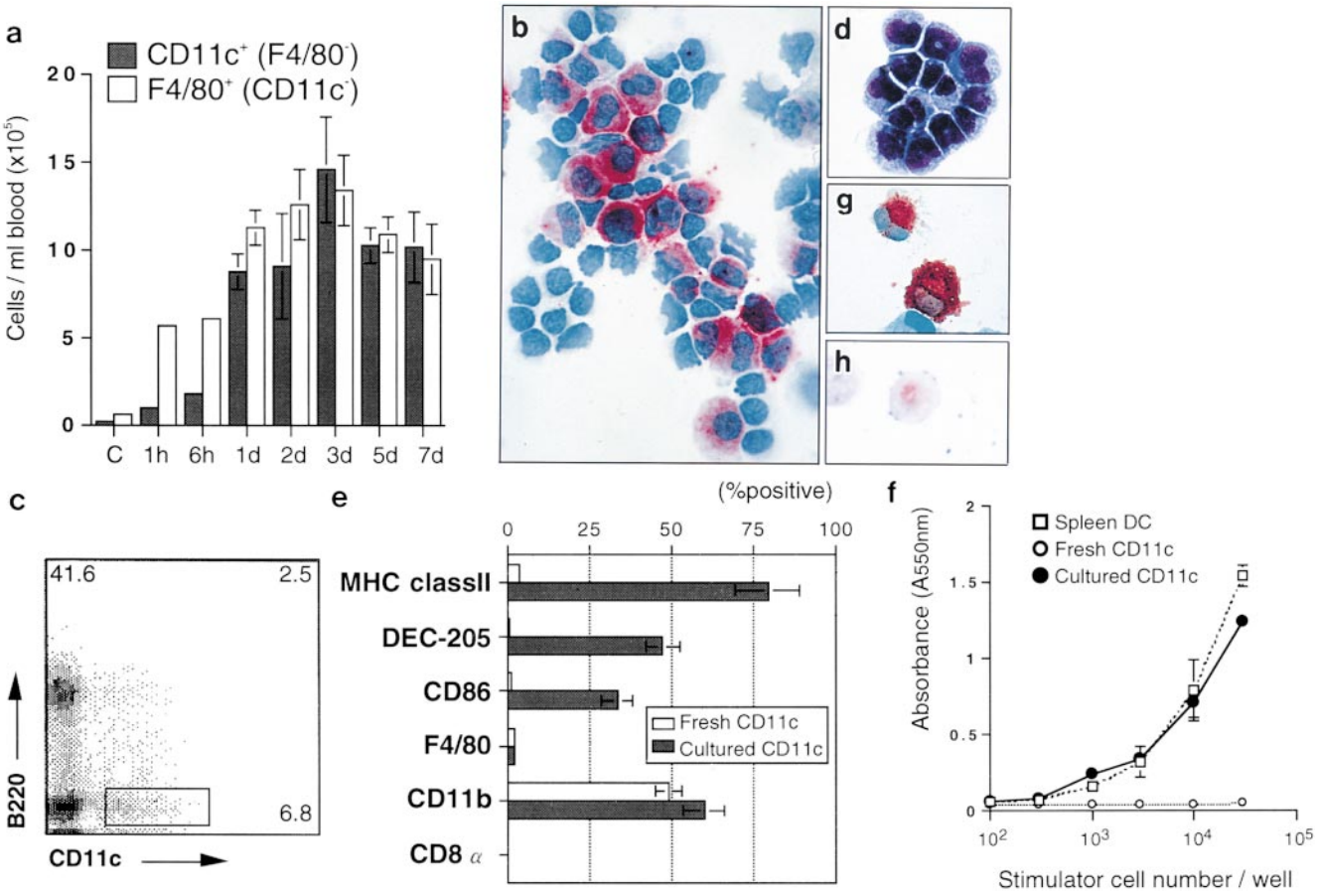

Figure 4. Emergence of CD11c$^+$ DC precursors in the circulation. (a) The absolute numbers of CD11c$^+$ and F4/80$^+$ cells were determined by multiplying the total PBL number per ml by the fraction of CD11c$^+$F4/80$^-$ and F4/80$^+$CD11c$^-$ population. (b) CD11c$^+$ PBLs (red) on day 7. (c) Gate for B220$^-$CD11c$^+$ subsets at day 5 by direct staining with PE-labeled anti-B220 mAb and FITC-labeled anti-CD11c mAb. (d) Freshly sorted B220$^-$CD11c$^+$ cells at day 5, stained with Giemsa. (e) Phenotype of freshly sorted and 10-d cultured B220$^-$CD11c$^+$ cells. (f) Primary allogeneic MLR of freshly sorted, 10-d cultured B220$^-$CD11c$^+$ cells, and spleen DCs. Representative data from three independent experiments. Mean = SD (n = 3). (g) MHC class II$^+$ (brown) 8-d cultured B220$^-$CD11c$^+$ cells. (h) *P. acnes* (brown)–laden CD11c$^+$ PBLs (day 1). Original magnifications: (b, d, g, and h) ×400.

(Fig. 1 b and Fig. 3 a), suggesting that CD11c$^+$ NPCs lodged in the granulomas acquired DEC-205 phenotype during maturation time. Notably, granuloma-derived CD11c$^+$ NPCs were negative for F4/80 (Fig. 3 d) throughout, indicating that they were distinct from Kupffer cells, macrophages, and mature monocytes.

Identification of Circulating DC Precursors. Expansion of CD11c$^+$ cells (Fig. 3 b) at granulomatous sites (Fig. 3 a) presumably depended on recruitment of CD11c$^+$ cells from the circulation. CD11c$^+$ cells were not found in the blood in the steady state, but rapidly increased to a peak level (15–20%) by day 1 of infection (Fig. 4, a and b). As

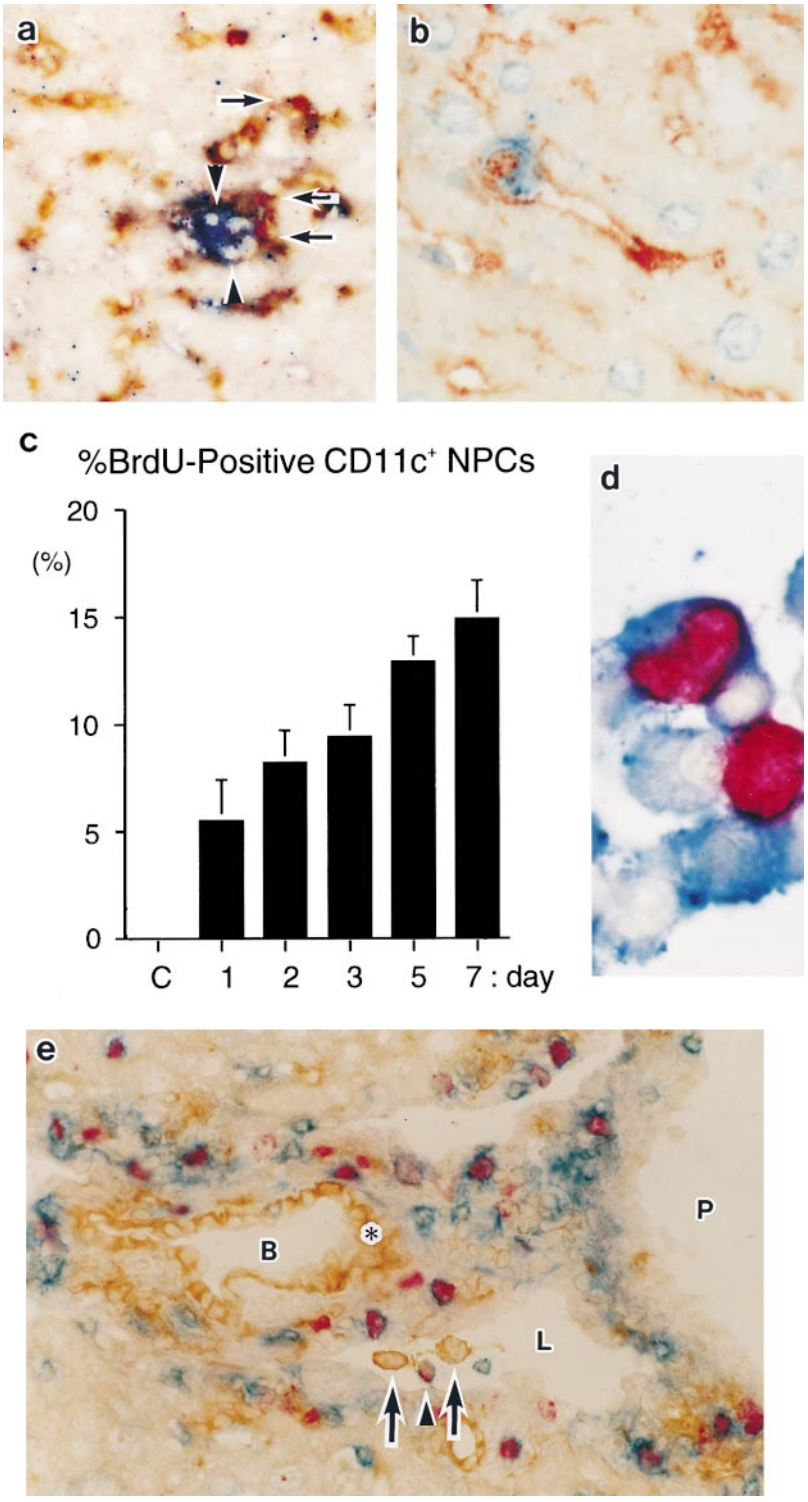

Figure 5. Entry, proliferation, and exit of DCs in the liver. (a) Primary cell cluster between CD11c$^+$ cells (arrowheads; blue) and *P. acnes* (red)–laden F4/80$^+$ cells (arrows; brown) in the sinusoidal wall (1 h). (b) *P. acnes* (red)–laden CD11c$^+$ cells (blue) in the sinusoid (6 h). (c) The labeling index of CD11c$^+$ NPCs by 1 h BrdU labeling. (d) Cytosmears of BrdU$^+$ (red) CD11c$^+$ (blue) NPCs on day 4. (e) DEC205$^+$DC (arrows; brown) as well as BrdU$^+$(red) CD4$^+$(blue) cells (arrowheads) leave the liver via dilated afferent lymphatics (day 7). Original magnifications: (a, b, d, and e) ×400. B, bile duct; P, portal vein; L, lymphatic; asterisk, nonspecific staining of bile ducts.

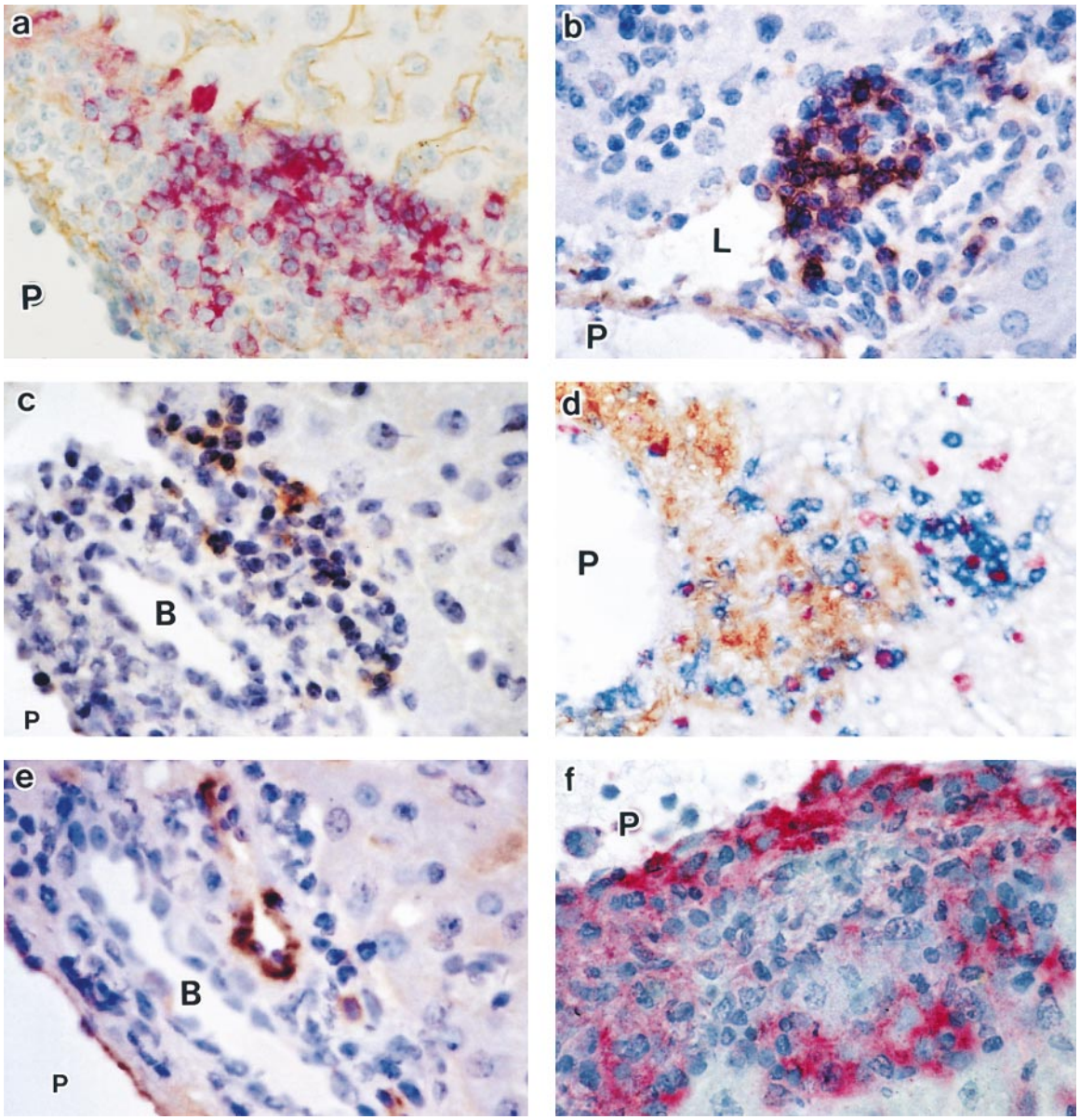

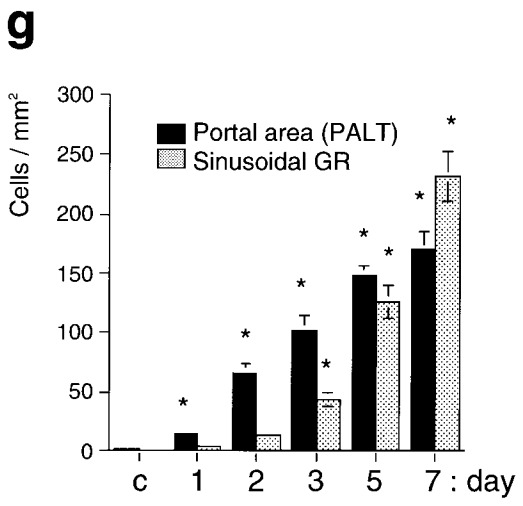

Figure 6. Formation of PALT. (a–f) Immunohistochemistry for B220 (a, red; type IV collagen, brown), FDC-M1 (b, brown), CR1 (c, brown), CD4 (d, blue; DEC205, brown; BrdU, red), PNAd (e, brown), and MOMA-1 (f, red) in PALT (day 7). Original magnifications: ×400. B, bile duct; P, portal vein; L, lymphatic. (g) Kinetics of $BrdU^{+}CD4^{+}$ cells in PALT and the sinusoidal granuloma (GR). Mean ± SD ($n = 6$). Asterisk, $P < 0.05$.

blood $CD11c^+$ cells were negative for F4/80, CD3ε, Gr-1, and a pan NK cell marker (data not shown), but had low levels of B220 (Fig. 4 c), we sorted $B220^-CD11c^+$ cells from PBLs at day 5 (Fig. 4 c). Freshly isolated $B220^-CD11c^+$ cells exhibited monocyte-like morphology (Fig. 4 d), and possessed neither the phenotypic markers of DCs, such as MHC class II, DEC-205, and CD86 (Fig. 4 e) nor DC function in allostimulation assays (Fig. 4 f). However, when $B220^-CD11c^+$ cells were cultured with GM-CSF alone for 5 d, and subsequently incubated with GM-CSF and TNF-α on type I collagen-coated plates for 3–4 d, they expressed the phenotype of DCs (Fig. 4, e and g) and acquired functional alloantigen-presenting capability (Fig. 4 f). These observations indicate that blood $B220^-CD11c^+$ cells represent DC precursors. In addition, ~10% of freshly isolated blood $B220^-CD11c^+$ cells at day 1 were positive for *P. acnes* as evidenced by immunostaining of cytosmears (Fig. 4 h), indicating that these cells also had phagocytic capability.

These $CD11c^+$ DC precursors may migrate to the perisinusoidal space from an early time and inhabit the developing granulomas being surrounded by *P. acnes*–laden macrophages (Fig. 5 a). Occasionally, *P. acnes*–laden $CD11c^+$ DCs were also detected in the sinusoidal area (Fig. 5 b), which is considered to be the site of DC entry. Some recruited $CD11c^+$ DCs possessed proliferating capability in the liver (Fig. 5, c and d). Altogether, we propose that blood $F4/80^-B220^-DEC\text{-}205^-CD11c^+$ cells are DC precursors, which enter the liver and gradually mature into functional MHC class $II^+DEC\text{-}205^+CD11c^+$ antigen-presenting cells within granulomas. Subsequently, DCs may undergo translocation from the liver to the hepatic lymph (13). $DEC\text{-}205^+$ DCs were found within the afferent lymphatics located in the portal area (Fig. 5 e), suggesting this area to be the site of DC exit.

Formation of PALT. Immunohistochemistry revealed that the *P. acnes*–induced portal infiltrate contained $B220^+$ B cell aggregations (Fig. 6 a), which were rarely seen in the sinusoidal area. Follicular DC (FDC)-reactive markers (29), $FDC\text{-}M1^+$ and $CR1^+$ cells, were also found in these portal B cell aggregates (Fig. 6, b and c) like B cell follicles, although typical germinal centers were not observed. In addition, $CD4^+$ T cells were found between B cell follicles and bile ducts (Fig. 6 d). The pattern was distinct from $CD4^+$ T cells in sinusoidal granulomas, which localized in the periphery of the granuloma (Fig. 1 c). The portal $CD4^+$ T cell clusters were associated with high endothelial venule (HEV)-like vessels as revealed by PNAd (30) staining (Fig. 6 e). On the outer rim of these B and T foci, macrophages were recognized by MOMA-1 (Fig. 6 f), ER-TR9, and antisialoadhesin Ab (data not shown). Accordingly, the portal infiltrates actually resembled the organization of lymphoid tissue in peripheral LNs, which contain B cell follicles, T cell areas, and macrophages. Therefore, *P. acnes* administration induced "tertiary" portal lymphoid tissue as well as sinusoidal granulomas.

The relationship between sinusoidal granulomas and the portal lymphoid tissues was examined by in situ BrdU staining. Although $BrdU^+CD4^+$ T cells were not detected within the developing granuloma until 3 d after *P. acnes* in-

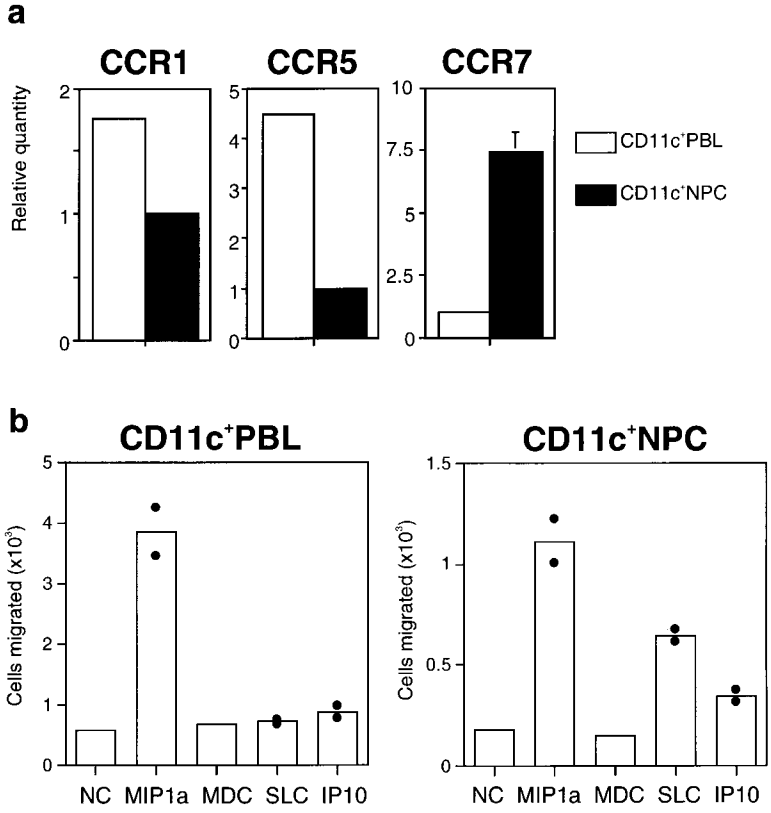

Figure 7. Migration potentials of DC precursors and liver DCs. (a) Real-time quantitative PCR analysis of chemokine receptor mRNA expressions on freshly isolated blood and liver $CD11c^+$ cells from *P. acnes*–primed mice at day 7. Each amount was normalized to the level of each glyceraldehyde-3-phosphate dehydrogenase. The final relative values were expressed relative to the calibrators; normalized amount of NPCs for CCR1 and CCR5, and of PBLs for CCR7. (b) Chemotaxis of freshly isolated blood and liver $CD11c^+$ cells at day 7. NC, medium alone as negative control. Representative data from three independent experiments. Mean ± SD ($n = 3$).

jection, such cells were already observed in the portal area from day 1 (Fig. 6 g). This indicates that $CD4^+$ T cell proliferation first occurred in the portal lymphoid tissues followed by the sinusoidal granulomatous areas. These observations suggested that the portal area was the primary site of immune responses to *P. acnes* locally in the liver, whereas the sinusoidal area appeared to be an effector site. We therefore propose here the concept that PALT plays a pivotal role in the immune response in an inflamed liver.

Migration Potential of DC Precursors and Liver DCs. On the presumption that transmigration of DCs was chemokine mediated, we examined chemokine receptor mRNA expression in freshly isolated blood and liver $CD11c^+$ cells and their migration potential. Blood $CD11c^+$ DC precursors predominantly expressed CCR1 and CCR5, whereas these receptors were downregulated in liver $CD11c^+$ cells. Only CCR7 was upregulated in liver $CD11c^+$ cells compared with blood DC precursors (Fig. 7 a). In chemotaxis assays, blood $CD11c^+$ DC precursors showed a significant chemotactic response toward MIP-1α, and had a weak response to SLC. In contrast, liver $CD11c^+$ cells acquired a migratory capacity toward SLC, although they still responded to MIP-1α (Fig. 7 b).

MIP-1α was weakly expressed in the sinusoidal endothelial cells and Kupffer cells in untreated liver, but was produced at high levels in the sinusoidal granulomas of inflamed liver (20; Fig. 8 a). On the other hand, SLC was constitutively produced by the portal lymphatic endothelia (31) and connective tissue stroma (Fig. 8 b). Furthermore, the expression levels of SLC mRNA in the liver were significantly increased after *P. acnes* injection (Fig. 8 c).

Chemokine Regulation of DC Precursor Trafficking into the Liver. To test whether blood DC precursors actually enter the liver, we adoptively transferred blood $CD11c^+$ cells derived from Ly5.2 mice into *P. acnes*–primed recipient congeneic (Ly5.1) mice. There seem to be at least two steps in DC trafficking into the liver. The first step was immediately after transfer (1 h) with $CD11c^+$ cells located predominantly in the sinusoidal granulomatous area (Fig. 9, a and b). The second step began 6 h after transfer with a significant increase in $CD11c^+$ cells in the portal area (Fig. 9 a). These DC precursors preferentially accumulated in the T cell area (Fig. 9 c), but not in the B cell follicle (Fig. 9 d) of PALT. $CD11c^+$ cells were also located in the paracortex of the hepatic LNs (Fig. 9 e) by 24 h, indicating that some of them underwent a sinusoid-lymph translocation and accumulated in the T cell area of the regional LNs (13). We next injected the recipient mice with neutralizing anti–MIP-1α pAb just before cell transfer. This inhibited trafficking of $CD11c^+$ DC precursors almost completely within all compartments in the liver (Fig. 9 a). Presumably, this was due to a failure of at least the first step of DC precursor migration. Thus, MIP-1α plays crucial roles in blood DC precursor trafficking into the liver. On the other hand, anti-SLC pAb

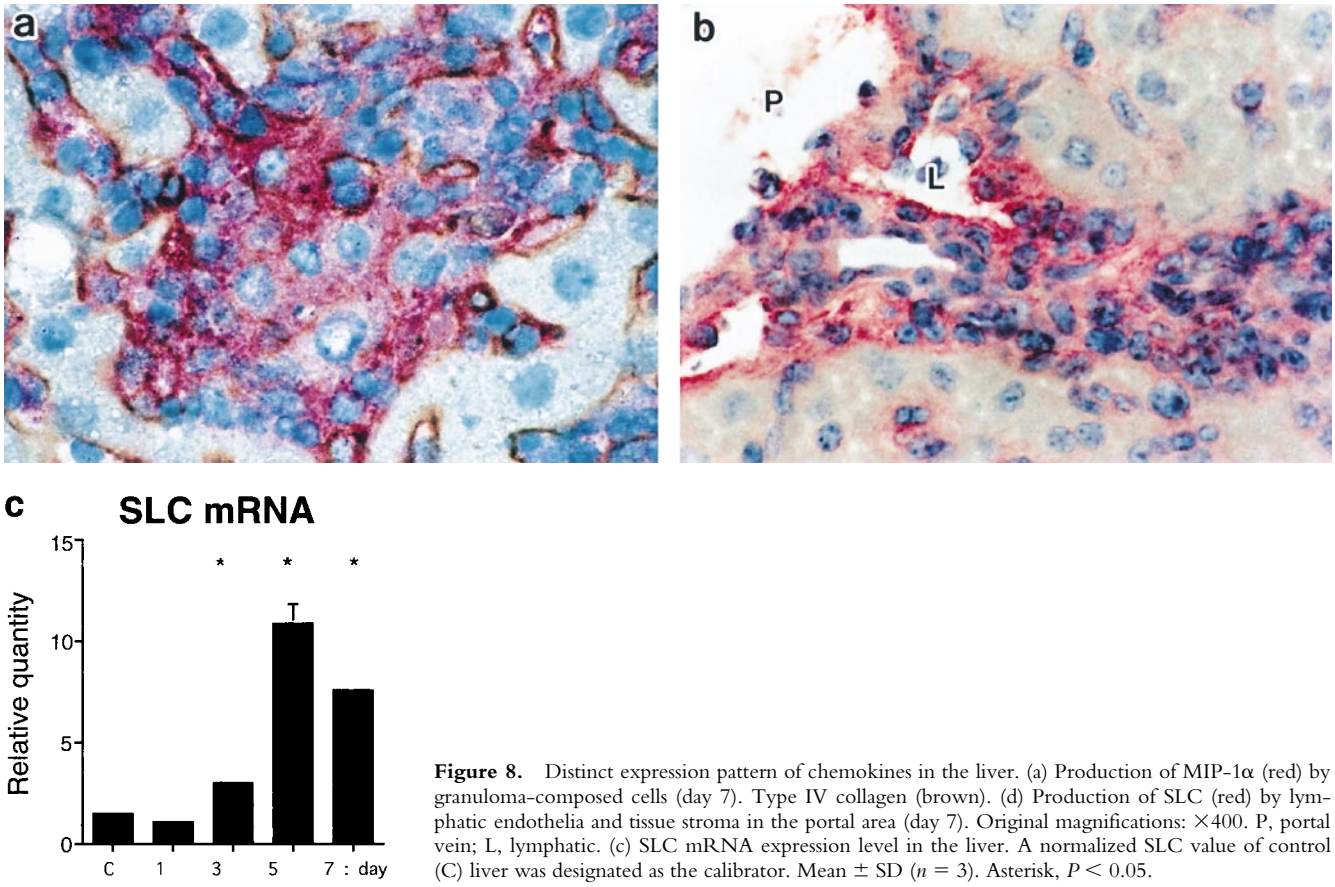

Figure 8. Distinct expression pattern of chemokines in the liver. (a) Production of MIP-1α (red) by granuloma-composed cells (day 7). Type IV collagen (brown). (d) Production of SLC (red) by lymphatic endothelia and tissue stroma in the portal area (day 7). Original magnifications: ×400. P, portal vein; L, lymphatic. (c) SLC mRNA expression level in the liver. A normalized SLC value of control (C) liver was designated as the calibrator. Mean ± SD ($n = 3$). Asterisk, $P < 0.05$.

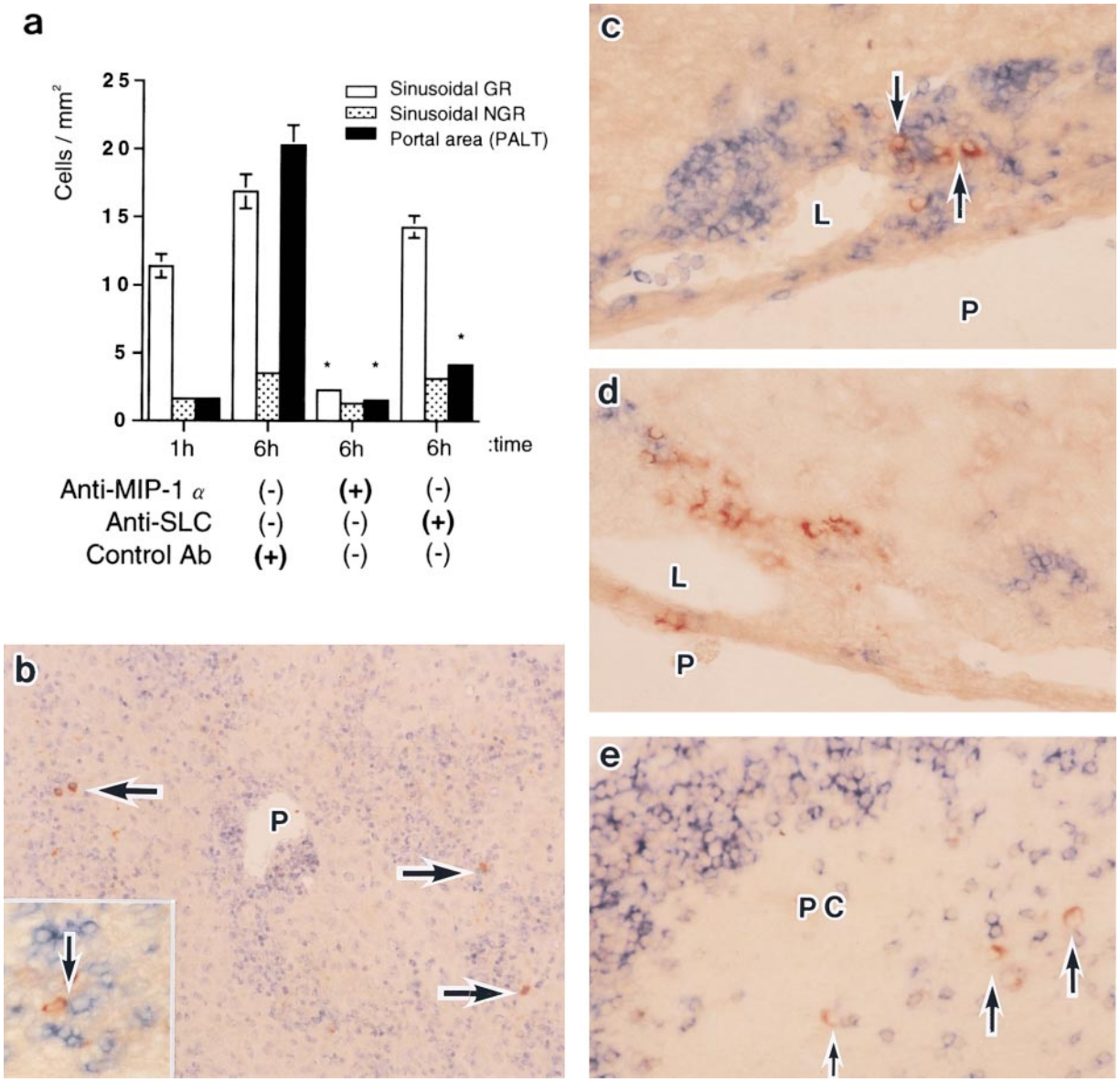

Figure 9. Chemokines regulate DC precursor trafficking into the liver. (a) Effect of anti–MIP-1α and anti-SLC pAbs on DC trafficking. 15 mm^2 of stained recipient cryosections were examined for the presence of donor cells within the sinusoidal granulomatous (GR), sinusoidal nongranulomatous (NGR), and PALT areas. Representative data from three independent experiments. Mean ± SD ($n = 3$). Asterisk, $P < 0.05$. (b–e) Donor (Ly5.2)-derived $CD11c^+$ cells (brown) in the sinusoidal granulomas (b, arrows; 1 h), the portal area (c and d, arrows; 6 h), and the paracortex in the hepatic LN (e, arrows; 24 h). B220 (d and e) or CD4 (b, inset, and c; blue). Original magnifications: (b) ×100; (b, inset) ×400; (c–e) ×200. P, portal vein; L, lymphatics; PC, paracortex.

injection showed almost no effect on the entry of DC precursors into the granulomatous area. Anti-SLC pAb did inhibit accumulation of $CD11c^+$ cells in the portal areas (Fig. 9 a). This suggests a selective blockade of the second migratory step of recruited DCs by anti-SLC pAb.

SLC Regulates Trafficking of DCs in Forming PALT. To define the biological role of SLC in granuloma formation, we investigated the effect of anti-SLC pAb on granuloma-associated liver injury. Mice were injected with anti-SLC pAb 0 and 2 d after *P. acnes* treatment. At day 7, anti-SLC pAb unexpectedly enhanced sinusoidal granuloma formation and hepatocellular damage (Fig. 10, a and b). In some cases, limited hepatocellular necrosis was observed surrounding the granulomatous area (Fig. 10 a). $CD11c^+$ NPCs were increased in number by treatment with anti-SLC pAb (Fig. 10 c), but they decreased in the portal area. This may be due to an interference with movement of $CD11c^+$ DCs into the portal area, but without any affect on the entry of blood $CD11c^+$ DC precursor into the liver sinusoid. Thus, $CD11c^+$ cells selectively increased in number in the sinusoidal granulomatous area and sometimes at the margin of the necrotic area. In contrast, $BrdU^+$ and $B220^+$ cells were reduced in number (Fig. 10 d) and the HEV-like vessels could not be seen in the portal area (data

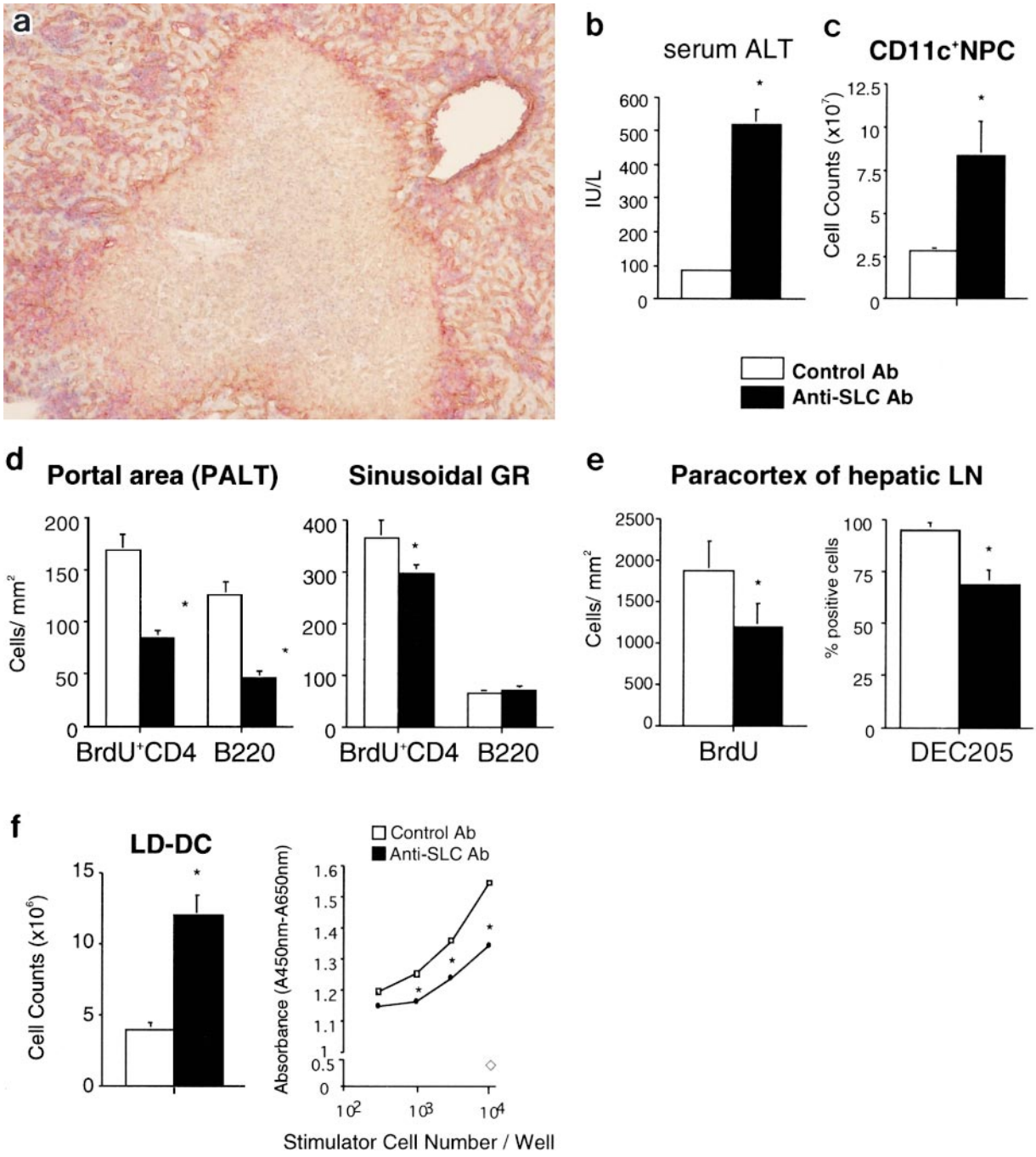

Figure 10. Effect of anti-SLC pAb on liver injury and PALT. (a) CD11c$^+$ cells (red) surround the necrotic area at 7 d after treatment with anti-SLC pAb. Type IV collagen (brown). Original magnification: ×100. (b) Serum ALT levels on day 7. (c) The absolute numbers of CD11c$^+$ NPCs. (d and e) The numbers of BrdU$^+$CD4$^+$ and B220$^+$ cells in the PALT and sinusoidal granulomatous (GR) area, and BrdU$^+$ and DEC205$^+$ cells in the paracortex of hepatic LNs determined by 15 mm^2 stained cryosections on day 7. T cell area of hepatic LNs was defined by B220 or CD3ε staining. (f) The absolute numbers and primary allogeneic MLR of LD-DCs from anti-SLC pAb and control Ab–treated mice (day 7). Representative data from six independent experiments. Mean ± SD ($n = 3$). Asterisk, $P < 0.05$.

not shown), supporting the inhibitory role of anti-SLC pAb on induction of PALT. This means anti-SLC pAb treatment reduced PALT expansion, but enhanced sinusoidal granuloma formation. BrdU$^+$ and DEC-205$^+$ cells were also decreased in number in the T cell areas of hepatic LNs, after anti-SLC Ab treatment (Fig. 10 e), suggesting that mature DEC-205$^+$ DCs failed to migrate to the regional LNs via draining lymphatics and that naive CD4$^+$ T cells also failed to enter the LNs via HEVs from the circulation (6). As a consequence, cluster formation between mature DCs and naive T cells within PALT and regional LNs were decreased, leading to impaired primary T cell prolif-

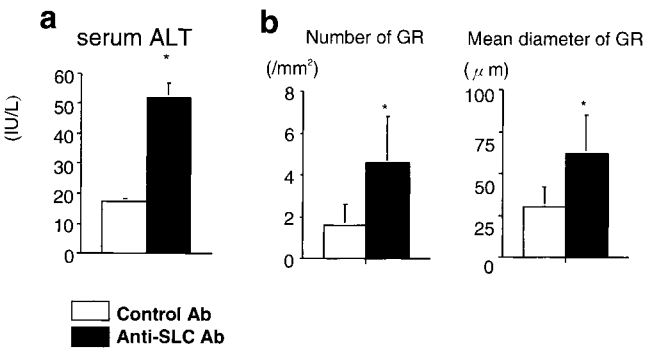

Figure 11. Anti-SLC pAb prolongs granuloma formation. (a) Serum ALT levels on day 28. (b) The number and the size of granuloma (GR) on day 28. Representative data from three independent experiments. Mean ± SD ($n = 6$). Asterisk, $P < 0.05$.

erative responses. Most of the granuloma-derived LD DCs obtained from anti-SLC pAb–treated liver showed low allostimulatory capability (Fig. 10 f), suggesting that immobilized DCs within granulomas did not undergo functional maturation. The reduction in number of $BrdU^+CD4^+$ T cells in the sinusoidal area (Fig. 10 d) also supported this idea. Therefore, effective immune responses were impaired not only locally but also at regional LN levels.

1 mo after *P. acnes* injection, granulomas disappeared almost completely in control Ab-treated mice, but persisted in anti-SLC pAb–treated mice together with elevation of serum ALT level (Fig. 11, a and b). Collectively in summary, anti-SLC pAb immobilized $CCR7^+CD11c^+$ DC in the granuloma sites, impaired the capacity of the host immune responses to eliminate *P. acnes*, and resulted in the persistence of granulomas.

Emergence of Inflammation-associated Circulating $CD11c^+$ DC Precursors in Monocyte-deficient Mice. Finally, to establish that $CD11c^+$ DC precursors are not derived from monocytes, we investigated whether $CD11c^+$ cells appear both in the circulation and in the hepatic granulomas using op/op mice that lack M-CSF–dependent monocytes. $F4/80^-CD11c^+$ cells defined as DC precursors appeared in the circulation, even in op/op mice (Fig. 12 a). Although the total number of $CD11c^+$ cells was decreased in op/op mice, their proportion in the blood was similar to that of control littermate mice. Moreover, *P. acnes* injection induced granulomas containing $CD11c^+$ cells in situ even in op/op mice, although their number and the size of the granulomas were decreased (Fig. 12, b and c). These results support the notion that $F4/80^-CD11c^+$ DC precursors identified in this study originate from cells distinct from monocytes.

Discussion

Granuloma formation is a hallmark of persistent infection (32). *P. acnes* is considered to be the cause of sarcoidosis (33). Experimentally, this anaerobic bacterium also leads to granulomas in the lung and liver (20, 33). Our data indicate that granuloma formation involves not only a macrophage-based component but also a DC-induced adoptive response.

We have demonstrated in this study murine DC precursors, defined as $CD11c^+F4/80^-DEC\text{-}205^-MHC\ class\ II^-$ cells, in the peripheral blood, which appeared rapidly after *P. acnes* injection. Peripheral blood DC precursors can be functionally classified into three groups in human $CD11c^+HLA\text{-}DR^{high}$ DCs (1, 34, 35), $CD11c^-HLA\text{-}DR^{high}$ DCs (1, 36, 37), and monocytes (1, 38). In mice, in contrast, recognition of DC precursors in the circulation has been difficult because they are MHC class II negative (10, 39; Fig. 4 e). Recently, mouse inflammatory monocytes were shown to differentiate into DCs after several days in vivo (40). In this experimental situation, neither monocyte-derived DC precursors nor monocytes expressed CD11c. In contrast, in this study, $CD11c^+$ cells rapidly appeared both in the circulation and in the liver from an early stage (within 6 h) after *P. acnes* injection (Fig. 3 b and Fig. 4 a), and some of the $CD11c^+$ cells in the liver showed significant proliferating activities (Fig. 5 c). Mono-

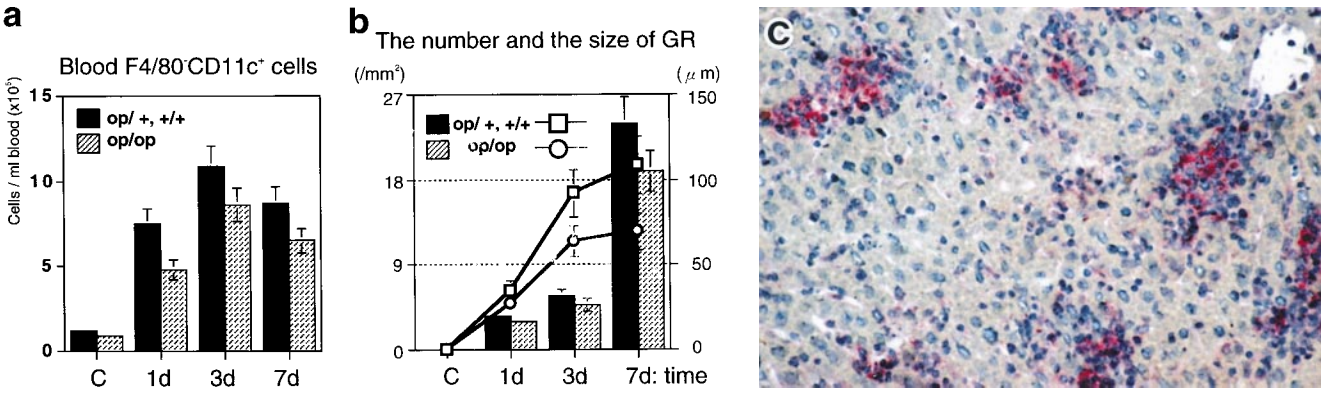

Figure 12. Emergence of $CD11c^+$ cells both in the circulation and in the liver in *P. acnes*–primed monocyte-deficient mice. (a) The absolute numbers of $CD11c^+F4/80^-$ PBLs. (b) The number (bars, left y axis) and the size (lines, right y axis) of granuloma (GR). Mean ± SD ($n = 3$). (c) $CD11c^+$ cells (red) in a granuloma of op/op mouse on day 7. Original magnifications: ×100. All granulomas present in the *P. acnes*–primed op/op mice were $CD11c^+$ during disease course.

cytes are considered to be nonproliferating stage cells, and monocytes cultured to undergo differentiation into DCs usually do not contain cycling cells (41). $F4/80^+CD11c^-$ cells also emerged in the circulation, but these cells never expressed CD11c throughout (Fig. 4 a), similar to the above study (40). In monocyte-deficient op/op mice, blood $CD11c^+$ cells rapidly appeared 1 d after *P. acnes* injection (Fig. 12 a) and these cells constituted granuloma (Fig. 12, b and c). Although *P. acnes* injection may induce some cytokines (20) that substitute for M-CSF activity even in op/op mice (42, 43), 24 h is too short and very unlikely for these cytokines to differentiate a large number of monocytes into $CD11c^+$ DC precursors. We therefore consider that $CD11c^+$ precursors are distinct from inflammatory monocytes (40), and blood $F4/80^+CD11c^-$ cells, on the other hand, are activated monocytes.

Interaction with endothelial cells is required for blood leukocytes to extravasate into tissues (5). Circulating DC precursors may also transmigrate through the sinusoidal wall in the liver to participate in granuloma formation. The sinusoidal wall contains several distinct cell types: endothelial cells, Kupffer cells, a few pit cells located in the hepatic sinusoid, and Ito cells in Disse's space. The sinusoidal wall is the principal site for capturing blood-borne microorganisms (44), and most inflammatory infiltrates, including *P. acnes*–induced granulomas, are initially formed in Disse's space (44, 45). Uniquely in the liver, Kupffer cells predominantly interact with blood-borne DCs (13) and enable them to extravasate through endothelial pores to enter Disse's space (46), then help them translocate into hepatic lymph (13). As Kupffer cell–derived MIP-1α may recruit circulating DC precursors (Fig. 7 b), interaction of DC precursors and *P. acnes*-laden Kupffer cells (Fig. 5 a) may initiate to form granuloma in Disse's space. Recruited $CD11c^+$ DC precursors themselves produce MIP-1α (data not shown) to induce another wave of DC precursor migration into the inflamed liver.

After entering the sinusoidal wall, DC precursors may undergo further maturational processes. Some DCs subsequently move through draining lymphatic pathways to regional hepatic LNs. During this migration, DCs must first pass the portal tract, as lymphatic capillaries are mostly located in this area (14). SLC on the lymphatic capillaries may attract DCs (Fig. 7 b) and induce PALT expansion. Part of the DCs remains within the sinusoidal developing granulomas. In association with the maturation of the retained DCs, proliferating $CD4^+$ T cells appear in granulomas (Fig. 1 c), suggesting that recently activated memory $CD4^+$ T cells home to the granulomatous areas from regional LNs via efferent lymphatics and circulation. MIP-1α, IFN-γ–inducible protein 10 (IP-10), and monokine induced by IFN-γ (Mig) may recruit $CCR5^+$ or $CXCR3^+$ Th1–type $CD4^+$ T cells into the liver (20). Thus, activated DCs maintain the local inflammatory reaction to sequester microorganisms within a granuloma consisting of clusters of DCs, macrophages, and $CD4^+$ T cells.

How do DCs migrate to the portal area? DCs may extravasate through the sinusoidal wall after binding to Kupffer cells. Two possible systems for transferring blood-borne antigens from the sinusoidal area to the portal area are possible. First, DC precursors may phagocytose antigens in the sinusoidal wall during interaction with Kupffer cells. This pattern is similar to that of M cells and subepithelial dome DCs in Peyer's patches (19, 47). As Disse's space is continuous with the tissue space of the portal area (48), after capturing antigens, activated DCs may extravasate and exit the hepatic lobule (Fig. 5 e). SLC produced in the portal area may attract these DCs, in addition to a passive movement due to the negative pressure produced by lymph flow (14). Delay of emergence of DC precursors in the portal area (Fig. 9 a) by anti-SLC pAb supports this interpretation. Hence, it is likely that DCs within Disse's space move from the sinusoidal unit to PALT. Second, antigens may be also transported in a free form in tissue fluid flowing through Disse's space from the sinusoidal area to the portal area.

Normally, cellular infiltration in the portal area is rather sparse. In contrast, increased "portal infiltration" has been described in pathological states (14). Therefore, PALT is an inducible structure similar to bronchus-associated lymphoid tissue (29). The liver is also a site for production of Ab, especially secretory IgA which is transported into bile duct. The location between bile duct and PALT resembles that between salivary gland and duct-associated lymphoid tissue (49). PALT may act as first line defense of the lymphatic pathway as well as sites of local immune induction. Moreover, the loss of PALT was accompanied by more advanced hepatocellular damage in the sinusoidal area (Fig. 10). These observations indicate that the balance between protective PALT and the injurious sinusoidal granuloma would determine the disease outcome.

In our model, the treatment with anti-SLC pAb inhibited the maturation of recruited DC precursors at granulomatous sites, although the number of DCs in the liver was increased. Once DC precursors enter the tissue, impairment of appropriate DC trafficking may exacerbate and prolongs disease course. These data suggest a need for DCs to form effective granulomas that clear infection, and suggest that inadequate DC function may cause chronic inflammation and less effective host resistance. By regulating the SLC–CCR7 interactions, DCs could be directed to the appropriate site such as PALT to initiate immune response. This should minimize the severity of the disease.

In conclusion, we have discovered inflammation-associated, circulating DC precursors probably distinct from the previously reported inflammatory monocytes. These precursors migrate into a peripheral site of inflammation as quickly as monocytes, mature within developing granulomas, and are likely to trigger the immune response. We have also established the existence of PALT that may form immune responses locally in the liver and affect the eventual outcome of liver injury. Chemokines regulate this DC trafficking, and thereby most likely contribute to local disease outcome. Our in vivo study could extend to other local tissues and suggests a role for DCs in chronic granulomatous inflammation.

We are very grateful to Dr. Joost J. Oppenheim (National Cancer Institute, Frederick, MD) for review before submission. We express our sincere gratitude for the generous gifts of mAbs to Dr. R.M. Steinman (M342), Dr. M.H. Kosco-Vilbois (FDC-M1), Dr. Y. Eishi (*P. acnes*), Dr. T. Kina (Ly5.2), and of op/op mice to Dr. M. Takeya. We thank Dr. H. Iizasa and Ms. N. Genda (Kyoritsu College of Pharmacy, Tokyo, Japan) for technical advice and assistance, and Mr. S. Fujita for animal surgical assistance.

This study was supported in part by a grant from Core Research and Evolutional Science and Technology (CREST), Japan Science and Technology Corporation.

Submitted: 28 June 2000
Revised: 30 August 2000
Accepted: 12 October 2000

References

1. Banchereau, J., and R.M. Steinman. 1998. Dendritic cells and the control of immunity. *Nature*. 392:245–252.
2. Dieu-Nosjean, M.C., A. Vicari, S. Lebecque, and C. Caux. 1999. Regulation of dendritic cell trafficking: a process that involves the participation of selective chemokines. *J. Leukoc. Biol*. 66:252–262.
3. McWilliam, A.S., S. Napoli, A.M. Marsh, F.L. Pemper, D.J. Nelson, C.L. Pimm, P.A. Stumbles, T.N.C. Wells, and P.G. Holt. 1996. Dendritic cells are recruited into the airway epithelium during the inflammatory response to a broad spectrum of stimuli. *J. Exp. Med*. 184:2429–2432.
4. Charbonnier, A-S., N. Kohrgruber, E. Kriehuber, G. Stingl, A. Rot, and D. Maurer. 1999. Macrophage inflammatory protein 3α is involved in the constitutive trafficking of epidermal Langerhans cells. *J. Exp. Med*. 190:1755–1767.
5. Robert, C., R.C. Fuhlbrigge, J.D. Kieffer, S. Ayehunie, R.O. Hynes, G. Cheng, S. Grabbe, U.H. von Andrian, and T.S. Kupper. 1999. Interaction of dendritic cells with skin endothelium: a new perspective of immunosurveillance. *J. Exp. Med*. 189:627–635.
6. Foster, R., A. Schubei, D. Breitfeld, E. Kremmer, I. Renner-Muller, E. Wolf, and M. Lipp. 1999. CCR7 coordinates the primary immune response by establishing functional microenvironments in secondary lymphoid organs. *Cell*. 99:23–33.
7. Gunn, M.D., S. Kyuwa, C. Tam, T. Kakiuchi, A. Matsuzawa, L.T. Williams, and H. Nakano. 1999. Mice lacking expression of secondary lymphoid organ chemokine have defect in lymphocyte homing and dendritic cell localization. *J. Exp. Med*. 189:451–460.
8. McWilliam, A.S., D. Nelson, J.A. Thomas, and P.G. Holt. 1996. Rapid dendritic cell recruitment is a hallmark of the acute inflammatory response at mucosal surface. *J. Exp. Med*. 179:1331–1336.
9. Larsen, C.P., P.J. Morris, and J.M. Austyn. 1990. Migration of dendritic leukocytes from cardiac allografts into host spleens: a novel route for initiation of rejection. *J. Exp. Med*. 171:307–314.
10. Roake, J.A., A.S. Rao, P.J. Morris, C.P. Larsen, D.F. Hankins, and J.M. Austyn. 1995. Systemic lipopolysaccharide recruits dendritic cell progenitors to nonlymphoid tissues. *Transplantation*. 59:1319–1324.
11. Roake, J.A., A.S. Rao, P.J. Morris, C.P. Larsen, D.H. Hankins, and J.M. Austyn. 1995. Dendritic cell loss from nonlymphoid tissues after systemic administration of lipopolysaccharide, tumor necrosis factor, and interleukin 1. *J. Exp. Med*. 181:2237–2247.
12. Matsuno, K., T. Ezaki, S. Kudo, and Y. Uehara. 1996. A life stage of particle-laden rat dendritic cells in vivo: their terminal division, active phagocytosis, and translocation from the liver to the draining lymph. *J. Exp. Med*. 183:1865–1878.
13. Kudo, S., K. Matsuno, T. Ezaki, and M. Ogawa. 1997. A novel migration pathway for rat dendritic cells from the blood: hepatic sinusoids-lymph translocation. *J. Exp. Med*. 185:777–784.
14. Matsuno, K., and T. Ezaki. 2000. Dendritic cell dynamics in the liver and hepatic lymph. *Int. Rev. Cytol*. 197:83–135.
15. Sallusto, F., A. Lanzavecchia, and C. Mackay. 1998. Chemokines and chemokine receptors in T-cell priming and Th1/Th2-mediated responses. *Immunol. Today*. 19:568–574.
16. Cyster, J.G. 1999. Chemokines and cell migration in secondary lymphoid organs. *Science*. 286:2098–2102.
17. Melchers, F., A.G. Rolink, and C. Schaniel. 1999. The role of chemokines in regulating cell migration during humoral immune responses. *Cell*. 99:351–354.
18. Randolph, D.A., G. Huang, C.J.L. Carruthers, L.E. Bromley, and D.A. Chaplin. 1999. The role of CCR7 in TH1 and TH2 cell localization and delivery of B cell help in vivo. *Science*. 286:2159–2162.
19. Iwasaki, A., and B.L. Kelsall. 2000. Localization of distinct Peyer's patch dendritic cell subsets and their recruitment by chemokines macrophage inflammatory protein (MIP)-3α, MIP-3β, and secondary lymphoid organ chemokine. *J. Exp. Med*. 191:1381–1393.
20. Yoneyama, H., A. Harada, T. Imai, M. Baba, O. Yoshie, Y. Zhang, H. Higashi, M. Murai, H. Asakura, and K. Matsushima. 1998. Pivotal role of TARC, a CC chemokine, in bacteria-induced fulminant hepatic failure in mice. *J. Clin. Invest*. 102:1933–1941.
21. Takahashi, K., M. Naito, L.D. Shultz, S.-I. Hayashi, and S.-I. Nishikawa. 1993. Differentiation of dendritic cell populations in macrophage colony-stimulating factor-deficient mice homozygous for osteopetrosis (op) mutation. *J. Leukoc. Biol*. 53: 19–28.
22. Takahashi, K., M. Naito, S. Umeda, and L.D. Shultz. 1994. The role of macrophage colony-stimulating factor in hepatic glucan-induced granuloma formation in the osteopetrosis mutant mouse defective in the production of macrophage colony-stimulating factor. *Am. J. Pathol*. 144:1381–1392.
23. Murai, M., H. Yoneyama, A. Harada, Y. Zhang, C. Vestergaard, B. Guo, K. Suzuki, H. Asakura, and K. Matsushima. 1999. Active participation of $CCR5^+CD8^+$ T lymphocytes in the pathogenesis of liver injury in graft-versus-host disease. *J. Clin. Invest*. 104:49–57.
24. Ogata, M., Y. Zhang, Y. Wang, M. Itakura, Y-Y. Zhang, A. Harada, S. Hashimoto, and K. Matsushima. 1999. Chemotactic response toward chemokines and its regulation by transforming growth factor-β1 of murine bone marrow hematopoietic progenitor cell-derived different subset of dendritic cells. *Blood*. 93:3225–3252.

24a. Itakura, M., A. Tokuda, H. Kimura, S. Nagai, H. Yoneyama, N. Onai, S. Ishikawa, T. Kuriyama, and K. Matsushima. 2000. Blockade of secondary lymphoid-tissue chemokine (SLC) exacerbates *Propionobacterium acnes*-induced acute lung imflammation. *J. Immunol*. In press.

25. Kawada, N., T. Kuroki, K. Kobayashi, M. Inoue, K. Nakatani, K. Kaneda, and K. Nagata. 1996. Expression of heat-shock protein 47 in mouse liver. *Cell Tissue Res*. 284:341–

346.
26. Zhang, Y., Y. Zhang, Y. Wang, M. Ogata, S. Hashimoto, N. Onai, and K. Matsushima. 2000. Development of dendritic cells in vitro from murine fetal liver-derived lineage phenotype-negative *c-kit*$^+$ hematopoietic progenitor cells. *Blood*. 95:138–146.
27. Woo, J., L. Lu, A.S. Rao, Y. Li, V. Subbotin, T.E. Starzl, and A.W. Thomson. 1994. Isolation, phenotype, and allostimulatory activity of mouse liver dendritic cells. *Transplantation*. 58:484–491.
28. Naito, M., S. Umeda, T. Yamamoto, H. Moriyama, H. Umezu, G. Hasegawa, H. Usuda, L.D. Shultz, and K. Takahashi. 1996. Development, differentiation, and phenotypic heterogeneity of murine tissue macrophages. *J. Leukoc. Biol*. 59:133–138.
29. Chvatchlo, Y., M.H. Kosco-Vilbois, S. Herren, J. Lefort, and J.-Y. Bonnefoy. 1996. Germinal center formation and local immunoglobulin E (IgE) production in the lung after airway antigenic challenge. *J. Exp. Med*. 184:2353–2360.
30. Mebius, R.E., P.R. Streeter, J. Breve, A.M. Duijvestijn, and G. Kraal. 1991. The influence of afferent lymphatic vessel interruption on vascular addressin expression. *J. Cell Biol*. 115: 85–95.
31. Gunn, M.D., K. Tangemann, C. Tam, J.G. Cyster, S.D. Rosen, and L.T. Williams. 1998. A chemokine expressed in lymphoid high endothelial venules promotes the adhesion and chemotaxis of naive T lymphocytes. *Proc. Natl. Acad. Sci. USA*. 95:259–263.
32. Kunkel, S.L., N.W. Lukas, R.M. Strieter, and S.W. Chensue. 1998. Animal models of granulomatous inflammation. *Semin. Resp. Infect*. 13:221–228.
33. Ishige, I., Y. Usui, T. Takemura, and Y. Eishi. 1999. Quantitative PCR of mycobacterial and propionibacterial DNA in lymph nodes of Japanese patients with sarcoidosis. *Lancet*. 354:120–123.
34. O'Doherty, U., R.M. Steinman, M. Peng, P.U. Cameron, S. Gezelter, I. Kopeloff, W.J. Swiggard, M. Pope, and N. Bhardwaj. 1993. Dendritic cells freshly isolated from human blood express CD4 and mature into typical immunostimulatory dendritic cells after culture in monocyte-conditioned medium. *J. Exp. Med*. 178:1067–1078.
35. Grouard, G., I. Durand, L. Filgueira, J. Banchereau, and L. Yong-Jun. 1996. Dendritic cells capable of stimulating T cells in germinal centers. *Nature*. 384:364–367.
36. Grouard, G., M-C. Rissoan, L. Filgueira, I. Durand, J. Banchereau, and L. Yong-Jun. 1997. The enigmatic plasmacytoid T cells develop into dendritic cells with interleukin (IL)-3 and CD40-ligand. *J. Exp. Med*. 185:1101–1111.
37. Cella, M., D. Jarrossay, F. Facchetti, O. Alebardi, H. Nakajima, A. Lanzavecchia, and M. Colonna. 1999. Plasmacytoid monocytes migrate to inflamed lymph nodes and produce large amounts of type I interferon. *Nat. Med*. 5:919–923.
38. Randolph, G.J., S. Beaulieu, S. Lebecque, R.M. Steinman, and W.A. Muller. 1998. Differentiation of monocytes into dendritic cells in a model of transendothelial trafficking. *Science*. 282:480–483.
39. Inaba, K., R.M. Steinman, M.W. Pack, H. Aya, M. Inaba, T. Sudo, S. Wolpe, and G. Schuler. 1992. Identification of proliferating dendritic cell precursors in mouse blood. *J. Exp. Med*. 175:1157–1167.
40. Randolph, G.J., K. Inaba, D.F. Robbiani, R.M. Steinman, and W.A. Muller. 1999. Differentiation of phagocytic monocytes into lymph node dendritic cells in vivo. *Immunity*. 11: 753–761.
41. Fujii, S., K. Fujimoto, K. Shimizu, T. Ezaki, F. Kawano, K. Takatsuki, M. Kawakita, and K. Matsuno. 1999. Presentation of tumor antigens by phagocytic dendritic cell clusters generated from human CD34$^+$ hematopoietic progenitor cells: induction of autologous cytotoxic T lymphocytes against leukemic cells in acute myelogenous leukemia patients. *Cancer Res*. 59:2150–2158.
42. Myint, Y.Y., K. Miyakawa, M. Naito, L.D. Schultz, Y. Oike, K. Yamamura, and K. Takahashi. 1999. Granulocyte/macrophage colony-stimulating factor and interleukin-3 correct osteopetrosis in mice osteopetrosis mutation. *Am. J. Pathol*. 154:553–566.
43. Niida, S., M. Kaku, H. Amano, H. Yoshida, H. Kataoka, S. Nishikawa, K. Tanne, N. Maeda, S. Nishikawa, and H. Kodama. 1999. Vascular endothelial growth factor can substitute for macrophage colony–stimulating factor in the support of osteoclastic bone resorption. *J. Exp. Med*. 190:293–298.
44. David, H., and P. Reinke. 1987. The concept of the "perisinusoidal functional unit" of the liver - importance to pathological processes. *Exp. Pathol*. 32:193–224.
45. Tsuji, N., N. Kawada, K. Ikeda, H. Kinoshita, and K. Kaneda. 1997. Immunohistochemical and ultrastractural analyses of in situ activation of hepatic stellate cells around *Propionibacterium acnes*-induced granulomas in the rat liver. *J. Submicrosc. Cytol. Pathol*. 29:125–133.
46. Sato, T., H. Yamamoto, C. Sasaki, and K. Wake. 1998. Maturation of rat dendritic cells during intrahepatic translocation evaluated using monoclonal antibodies and electron microscopy. *Cell. Tissue Res*. 294:503–514.
47. Neutra, M.R., A. Frey, and J.-P. Kraehenbuhl. 1996. Epithelial M cells: gateways for mucosal infection and immunization. *Cell*. 86:345–348.
48. Heath, T., and S. Lowden. 1998. Pathways of interstitial fluid and lymph flow in the liver acinus of the sheep and mouse. *J. Anat*. 192:351–358.
49. Nair, P.N.R., and H.E. Schroeder. 1986. Duct-associated lymphoid tissue (DALT) of minor salivary glands and mucosal immunity. *Immunology*. 57:171–180.